Pharmaceutical Nanotechnology

Elaboration of PLLA-based superparamagnetic nanoparticles: Characterization, magnetic behaviour study and in vitro relaxivity evaluation

Misara Hamoudeh [a], Achraf Al Faraj [b], Emmanuelle Canet-Soulas [b], François Bessueille [c], Didier Léonard [c], Hatem Fessi [a,*]

[a] *LAGEP, Laboratoire d'Automatique et de Génie de Procédés, UMR CNRS 5007, Pharmaceutical Technology Department, Université Lyon1 (UCLB) - CPE-Lyon, Bat 308G, 43 Bd du 11 Nov 1918, 69622 Villeurbanne Cedex, France*
[b] *Université Lyon 1, CREATIS - LRMN, UMR CNRS 5220, CPE, La Doua, 43 Boulevard du 11 Novembre 1918, 69622 Villeurbanne Cedex, France*
[c] *UMR 5180 des Sciences Analytiques, Université Lyon1 (UCLB), Villeurbanne, France*

Abstract

Oleic acid-coated magnetite has been encapsulated in biocompatible magnetic nanoparticles (MNP) by a simple emulsion evaporation method. The different parameters influencing the particles size were studied. Between these parameters, the stirring speed and the polymer concentration were found to influence positively or negatively, respectively, the MNP size which varied between 320 and 1500 nm. The magnetite encapsulation efficacy was about than 90% yielding a high magnetite loading of up to 30% (w/w). X-ray diffraction showed that magnetite crystalline pattern was not modified after emulsification and solvent evaporation. The X-ray photoelectron spectroscopy (XPS) results indicated the presence of less than 0.1% of iron atoms at the nanoparticles surface. Vibration simple magnetometer (VSM) showed a superparamagnetic behaviour of the MNP and a saturation magnetization increasing with the increased magnetite amount used in formulation. Moreover, T_1 and T_2 relaxivities of MNP (4.7 T, 20 °C) were 1.7 ± 0.1 and $228.3 \pm 13.1 \, s^{-1} \, mM^{-1}$, respectively, rendering them in the same category of known negative contrast agents which shorten the T_2 relaxation time. Therefore, by using an appropriate anticancer drug in their formulation, these magnetic nanoparticles can present a promising mean for simultaneous tumor imaging, drug delivery and real time monitoring of therapeutic effect.
© 2007 Elsevier B.V. All rights reserved.

Keywords: Magnetic nanoparticles; Magnetic resonance imaging (MRI); Superparamagnetism; Vibration simple magnetism (VSM); Surface study; Relaxivity

1. Introduction

In recent years, polymer based magnetic nanoparticles (MNP) have gained an increasing interest in the field of medicine and biotechnology due to their various potential applications in hyperthermia (Kim et al., 2006), magnetic resonance imaging (Shieh et al., 2005), DNA separation (Chiang and Sung, 2006), drug targeting (Timko et al., 2006) and enzyme purification (Safaiikova et al., 2003). Numerous preparation strategies for magnetic carriers have been described including emulsion polymerization (Pich et al., 2005), suspension polymerization (Xie et al., 2004), dispersion polymerization (Ushakova et al., 2003), microemulsion polymerization (Deng et al., 2003), solvent diffusion (Lee et al., 2005) and solvent evaporation (Gomez-Lopera et al., 2001). Many polymers have been used to prepare these magnetic carriers as poly(vinyl alcohol) (Sindhu et al., 2006), polystyrene (Zheng et al., 2005), poly(vinyl pyrrolidone) (Maensiri et al., 2006), poly(aniline) (Kryszewski and Jeszka, 1998) and polyesters like poly(lactide) (PLLA) (Hu et al., 2006), poly(D,L-lactide-co-glycolide) (PLGA) (Lee et al., 2005) and poly epsilon caprolactone (PCL) (Hamoudeh and Fessi, 2006). The later polyesters are distinguished by their biocompatible and biodegradable properties accompanied by a relatively low toxicity rendering them approved by the FDA (Lin et al., 1986; Herrmann and Bodmeier, 1998). Their degradation and the consequent release of loaded drugs can be controlled by their molecular weight and crystallinity (Kwon et al., 2001; Lemoine et al., 1996).

---

* Corresponding author. Tel.: +33 4 72 43 18 93; fax: +33 4 72 43 16 82.
  E-mail address: fessi@lagep.univ-lyon1.fr (H. Fessi).

Between the different applications of MNP, magnetic resonance imaging (MRI) has interestingly widened over the last decade to become the preferred cross-sectional imaging modality in various pathologies. In MRI, superparamagnetic nanoparticles are used for their significant capacity to produce predominantly T_2 relaxation effect resulting in a signal reduction on T_2-weighted images (a negative contrast). This effect is induced by the resulting magnetic field heterogeneity around the particles and through which water molecules diffuse inducing dephasing of the proton magnetic moments and by consequence, a T_2 effective transverse relaxation shortening. Generally speaking, iron oxides crystals sized between 3 and 10 nm can be encapsulated within these MNP for standard or functionalized contrast agents applications (e.g. Endorem[®] and Sinerem[®], Guerbet, France).

Clinically used contrast agents for MRI are gadolinium chelates and superparamagnetic iron oxide based nanoparticles (SPION) (Wang et al., 2001; Weissleder et al., 1990). SPIONs have important advantages over gadolinium chelates: they have low toxicity; in some instances toxicities were reported at concentrations more than 100 fold above the clinically effective dosage (Wang et al., 2001) and furthermore, their detection limit in MRI is in the subnanomolar range exceeding Gd imaging by a factor of 100 (Weissleder et al., 1990). The last point is to be seriously taken into account from a dose related toxicity point of view (Go et al., 1993; Bonnemain, 1998).

One of the promising MNP applications in MRI can be the image-guided delivery of drug-loaded nanoparticles in clinical oncology. Different papers have reported an improvement in the treatment efficacy due to a MRI coupled monitoring (Pauser et al., 1997; Zielhuis et al., 2005a,b; Seppenwoolde et al., 2005). Indeed, the possibility to use MRI to visualize anticancer drug-loaded nanoparticles distribution in the tumor and its surrounding healthy tissues is very important because it leads to the next advantages (i) pre-imaging of the drug-free nanoparticles distribution (a tracer dose) to enable a further good prediction of tumor targeting (Roullin et al., 2002), (ii) monitoring during and after administration of the drug-loaded nanoparticles leading to more efficious treatment (Seppenwoolde et al., 2005).

Indeed, an ideal magnetic carrier should be biocompatible with a low toxicity. Therefore, due to their acceptable biocompatibility as mentioned above, polyester polymers have been frequently chosen to prepare magnetic carriers. Recently, different papers have described the synthesis of PLLA, PLGA, PCL, PACA, based magnetic nanoparticles and microparticles and designed to be charged with an anticancer drug for an image-guided drug delivery or magnetic targeting (Hafeli et al., 1994; Müller et al., 1996; Gomez-Lopera et al., 2001; Lee et al., 2005; Okassa et al., 2005; Hamoudeh and Fessi, 2006; Hu et al., 2006; Wassel et al., 2007). Although many research groups have studied the superparamagnetic behaviour of these iron oxide-loaded polyester-based carriers, however, up to our knowledge, the in vitro longitudinal (r_1) and the transverse (r_2) relaxivities of these polyester-based carriers have not yet been evaluated in a manner to validate their potential utilisation in further MRI applications.

In this context, the goal of our investigation is to prepare PLLA based magnetic nanoparticles with a narrow polydispersity and a high reproducible magnetite loading, to study their magnetic behaviour and finally to evaluate their in vitro r_1 and r_2 relaxivity.

Briefly, magnetite has been encapsulated within nanoparticles of poly L-lactide acid. The magnetic Fe_3O_4/polymer composite nanoparticles were prepared by a solvent evaporation method. Different experiments were conducted to study the principal preparation parameters influencing the nanoparticles size and the size distribution. Furthermore, various characterisation assays were performed involving surface charge determination, both transmission and scanning electron microscopy, X-ray diffraction, Fourier transformed infrared, X-ray photoelectron spectroscopy, magnetic properties and in vitro relaxivity.

2. Materials and methods

2.1. Materials

The PLLA polymer (Resomer Condensate L Mn 1900 (Mw = 6 kDa) was kindly supplied by Boehringer Ingelheim, Germany. Ferrous chloride ($FeCl_2 \cdot 4H_2O$), Ferric chloride ($FeCl_3 \cdot 6H_2O$), oleic acid, poly(vinyl alcohol) (PVA, Mw = 31 kDa, hydrolyzation degree = 88%), boric acid, potassium iodide and iodine were all products of Aldrich, France. Dichloromethane (DCM) and ammoniac solution (25%) were from Laurylab, France. Nitric acid (65%), hydrochloric acid (12 M) sodium hydroxide (1 M), and sulphuric acid (95%) were purchased from Carlo-erba, France.

2.2. Synthesis of oleic acid-coated magnetite

Briefly, 24.3 g of $FeCl_3 \cdot 6H_2O$ and 12.0 g of $FeCl_2 \cdot 4H_2O$ were dissolved in 50 ml of distilled water in a round-bottomed flask under nitrogen. Then, 40 ml of NH_4OH (25%) were added at 70–80 °C. This minimizes the oxidation of superparamagnetic magnetite Fe_3O_4 to ferromagnetic Fe_2O_3. After the precipitation of magnetite crystals, oleic acid (40%, w/w of formed magnetite) was added dropwise during 10 min, and the flask was heated for 30 min. Then, the temperature was increased up to 110 °C in order to evaporate water and ammonium excess. The black lump-like gel was separated by magnetic decantation and cooled to room temperature then washed several times with distilled water to remove the excess of oleic acid. After drying, a black powder was obtained.

2.3. Nanoparticles preparation

Magnetic nanoparticles MNP have been prepared using a simple emulsion evaporation method as described by Hamoudeh and Fessi (2006) with some modification. Oil-in-water emulsion consisted of:

- Organic phase: Different amounts of oleic acid-coated magnetite (see Table 1) were mixed with the polymer used

Table 1
Different formulas and magnetite encapsulation efficacy determination (formulas and magnetite determination were performed in triplicate)

Formula	Oleic acid-coated magnetite (mg)	PLLA (mg)	Theoretical magnetite loading %[a]	Experimental magnetite loading %[a] (ICP-AES)	Encapsulation efficacy (%)[b]	Saturation magnetism (Ms) (emu/g)
A	25	400	5.08	4.83	95	1.5
B	50	400	11.1	9.87	88.9	5.03
C	100	400	20	17.66	88.3	7.5
D	200	400	33.33	31.05	93.15	14

[a] The experimental and theoretical loading % concern the oleic acid-coated magnetite.

[b] Encapsulation efficacy % = 100 × (experimental magnetite loading %/theoretical magnetite loading %).

at different concentrations (1–5%, w/v) in dichloromethane (DCM). The mixture was then introduced into an ultrasonic device (Branson 2200, USA) to obtain a good dispersion of magnetite in the organic phase.

- Aqueous phase: Poly(vinyl alcohol) (PVA) was dissolved in a continuously stirred water at 40 °C and left to cooling. PVA was used at different percentages ranging from 0.5 to 4% (w/v). The organic phase was then added into the aqueous one under mechanical stirring (Ultraturax T25, IKA, Germany) at a defined stirring speed for 2 min. The stirring speed ranged between 6500 and 24,000 rpm corresponding to the lowest and highest given stirring speeds by the apparatus, respectively.

After emulsion obtaining, the DCM was evaporated by a rotative evaporator (R-144, Buchi, Switzerland) at 100 rpm for 15 min. The formed nanoparticles were separated by ultra-centrifugation (Beckman, USA) at 50,000 rpm for 10 min and then washed with water for several times to eliminate the PVA excess.

Finally, 1 ml of nanoparticles suspension was filled into 5 ml freeze-drying vials to be lyophilized. The freeze-drying of MNP was performed using a pilot freeze-dryer; Usifroid SMH45 (Usifroid, France). It consists mainly of 3 stainless steel shelf plates (3 m × 0.15 m), a coiled tube used as a condenser at −65 ± 5 °C and a vacuum pump. The conditions applied during the present study were: freezing for 2 h at −50 °C with a temperature ramp of 1 °C/min, sublimation at −40 °C and 60 μbar for 15 h and finally the secondary drying was carried out at 25 °C and 50 μbar for 4 h.

2.4. Magnetite loading and encapsulation efficacy determination

Magnetite content was determined by two separated methods.

2.4.1. Thermogravimetric analysis (TGA)

The analysis was carried out on a TA 2950 (TA instruments, USA). Samples were analyzed in closed Platinum cups at a temperature range of 30–1000 °C (heating rate 10 °C/min) in a nitrogen atmosphere (flux of 5 ml/min). At the end of heating cycle, the detected amount of mineral residuum reflects the magnetite content (experimental loading). To calculate the encapsulation efficacy, we used the theoretical magnetite loading being the used amount of magnetite per 100 mg of prepared

sample (theoretical loading, Table 1).

Magnetite encapsulation efficacy %

$$= 100 \times \frac{\text{experimental loading}}{\text{theoretical loading}}.$$

2.4.2. Inductively coupled plasma atomic emission spectrometer (ICP-AES)

The titration of iron was performed on a spectrometer of ARL 3580 (Thermo, USA). A sample of 20 mg of prepared nanoparticles was digested in a medium containing 1 volumes of H_2SO_4 (95%) and 2 volume of fuming HNO_3 (65%) to solubilize the iron oxide. The assay was linear between 0 and 20 μg/ml with a correlation coefficient of 0.999. The encapsulation efficacy was calculated by the same equation as in TGA assay.

2.5. Size determination

The size and the shape of the synthesized magnetite crystals were determined from TEM images. For MNP, the size was determined by photon correlation spectroscopy (PCS) using Zetasizer 3000 HSa (Malvern, England) at 25 °C. Each measurement was performed in triplicate.

2.6. Scanning electronic microscopy (SEM)

MNP suspensions were deposited on a metallic probe then metallized with gold/palladium with a cathodic pulverizer technics Hummer II (6 V, 10 mA). Imaging was realized on a FEG Hitachi S800 SEM at an accelerating voltage of 15 kV.

2.7. Transmission electronic microscopy (TEM)

Both synthesised magnetite (dried form) and MNP suspensions were visualised using a Philips CM120 TEM. For MNP, a drop of a dilute dispersion was deposited on a copper grid covered with a formal-carbon membrane.

2.8. X-ray diffraction (XRD)

Sample crystallization was studied by an X-ray diffractometry system (Siemens D500) operated with Cu Kα X radiation at 40 kV and 30 mA. The scans were conducted in the 2θ range from 25 to 65°. The identification of the magnetite was carried out by comparing the diffraction pattern of the sample with

library data in the powder diffraction files using Diffrac-plus software.

2.9. Fourier transformed infrared

The infrared spectra were recorded with a Unicam Mattson 5000 FT-IR Spectrometer at room temperature. The spectra were taken in KBr discs in the range of 3500–400 cm^{-1}.

2.10. Zeta potential determination

The electrical characteristics of magnetite, MNP and magnetite-free nanoparticles were analyzed by electrophoresis measurements as a function of pH using Malvern Zetasizer 3000HS$_A$ (England). In this assay, different solutions of NaCl (0.001 M) in NaOH or HCl at pH values ranging from 3 to 11 were prepared using a pH meter (Metller Toledo, France). Diluted suspensions of MNP were made in these solutions to determine the pH effect on the potential zeta of MNP.

2.11. X-ray photoelectron spectroscopy (XPS)

Surface analysis was carried out using a RIBER SIA 200 spectrometer. XPS analyses were performed for C 1s, O 1s, Fe 2p, Fe 2p3/2 and Fe 3p peaks using a non-monochromatized Al Kα X-ray source.

2.12. Determination of poly(vinyl alcohol)

The residual amount of PVA in the nanoparticles was determined using an iodine-borate colorimetric method (Zielhuis et al., 2005a,b) with some modification. The method involves the extraction of poly(vinyl alcohol) from the sample matrix into an aqueous phase, followed by the formation of a PVA–iodine–borate complex that can be detected by visible spectroscopy. The method consists of solubilizing PVA by destructing the nanoparticles (50 mg) with 2 ml of 1 M NaOH for 30 min at 90 °C. The resulting solution was neutralized with 1 M HCl. Then, 3 ml of a boric acid solution (3.7%, w/v) and 0.5 ml of an iodine solution (1.66% KI + 1.27% I$_2$ in distilled water) were added and the volume was adjusted to 10 ml with distilled water. Samples were analysed at 680 nm using a Cary 50 spectrophotometer (Varian, Australia) in triplicate. Known amounts of PVA added to 50 mg of PLLA were treated in the same way and used as standards. The correlation coefficient for the given standards of PVA was 0.988.

2.13. Vibration sample magnetometer

A VSM-BS2-11 Tesla was used to study the magnetic properties of synthesized magnetite and MNP. The field dependence of magnetization was recorded at 10 K and 300 K under different applied magnetic fields; the applied magnetic field ranged between 1.5 and −1.5 T, then from −1.5 to 1.5 T. The temperature dependence of the nanoparticles magnetization was also investigated as following: the sample was cooled down to 10 K at a magnetic field of 1.5 T, then measurements of the magnetic

moment at a series of intermediate temperatures were carried out up to 300 K.

2.14. In vitro MRI

In order to evaluate the longitudinal and the transverse relaxivities (r_1 and r_2, respectively) of MNP, a MRI study was performed on tubes containing a suspension of MNP at different dilutions in distilled water giving increasing iron concentrations (0, 0.05, 0.10, 0.15, 0.20, 0.25, 0.35, 0.5, 0.75 mM). The assays were conducted using a 4.7 T Bruker MR system at 25 °C and with a volumic coil of a 6 cm interior diameter.

For the measurement of T_1 relaxation times, 2D imaging with an inversion-recovery fast imaging with steady state precession (IR-FISP) sequence was obtained using the shortest possible TE (echo time) and TR (repetition time) (TR/TE = 4.6/2.3 with a bandwidth = 50 MHz) and an increasing inversion time starting from the shortest T_1 = 90.2 ms with 60 echos. T_1 was calculated automatically from the data analysis of the Bruker system using the equation: $Y = A + |C \times 1 – 2 \times e(-t/T_1)|$ where A is the absolute biais; C the signal intensity; T_1 is the spin lattice relaxation time.

For measurements of T_2 relaxation times, Multi Spin Multi Echo (MSME) sequences were obtained with a TR of 2000 ms and increasing TEs of 11.7, 25, 40, 60 and 75 ms. Using Image J software (NIH), T_2 was calculated using a simplex algorithm to fit the values from each slice in a T_2 stack to the exponential equation: $\Delta S_n = S_0 \exp^{-TE_n/T_2}$.

Relaxivities (r_1 and r_2) are generally defined as the slope of the linear regression generated from a plot of the measured relaxation rate ($1/T_i$, where $i = 1$, 2) versus the concentration of the particles. $(1/T_i) = (1/T_{i(0)}) + r_i[MNP]$ where T_i denotes the longitudinal (T_1) or transverse (T_2) relaxation times of a suspension containing the particles and $T_{i(0)}$ is the relaxation time of the solvent (water) without particles.

3. Results and discussion

3.1. Synthesis of oleic acid coated magnetite

The synthesized magnetite chemical structure was determined by X-ray diffraction. The results show clearly that it has the six characteristic diffraction peaks of standard Fe$_3$O$_4$ crystal (isometric-hexoctahedral crystal system) (Hamoudeh and Fessi, 2006). Furthermore, the size and the morphology of magnetic powder were characterized by TEM (Fig. 1A). The estimated size of magnetite crystals was around 12 nm being comparable to a reported value of 8 nm (Zheng et al., 2005). Magnetite crystals with a size generally less than 30 nm exhibit superparamagnetism (Gupta and Gupta, 2005). Thus, the prepared magnetite were expected to have superparamagnetic properties and therefore, the superparamagnetic profile of the synthesized magnetite was verified by recording the magnetization behaviour with VSM. A typical plot of magnetization was conducted versus applied magnetic field (M–H loop) at 300 K. The magnetization curve exhibited neither remanence nor coercivity showing that magnetite crystals have a superparamagnetic behaviour with a
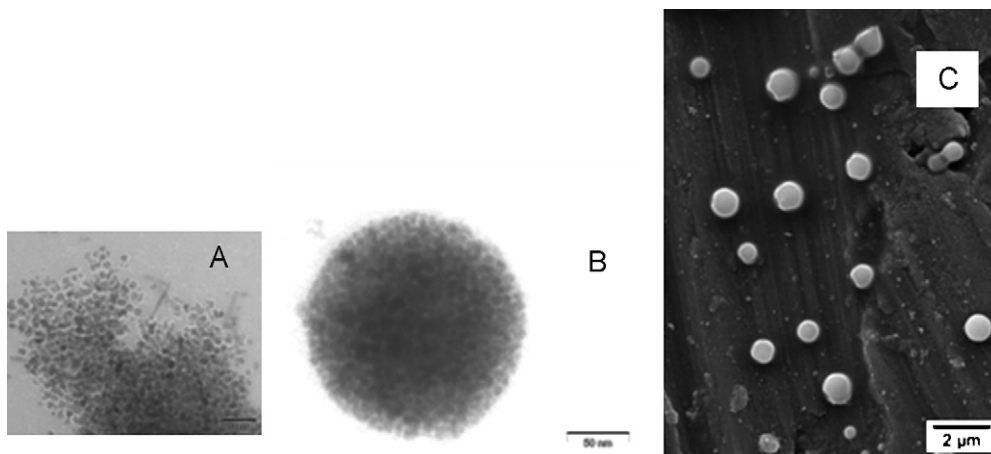
Fig. 1. (A) TEM micrograph on magnetite (bar = 100 nm). (B) TEM micrograph of MNP (formula C, stirring speed = 22,000 rpm; PVA concentration = 0.5%, w/v; PLLA concentration = 4%, w/v) (bar = 50 nm). (C) SEM micrograph of MNP (formula C, stirring speed = 17,500 rpm; PVA concentration = 0.5%, w/v; PLLA concentration = 4%, w/v) (bar = 2 μm).

saturation magnetization (Ms) of 70 emu/g which is relatively near the value reported by Xu et al. (2002). However, the saturation magnetization of oleic acid coated-magnetite was lesser (43 emu/g) as shown in our previous paper (Hamoudeh and Fessi, 2006) which was explained by the fact that the oleic acid (about 30%, w/w as confirmed by TGA) can be considered as a magnetically dead layer at the magnetite surface as shown by Kim et al. (2001).

3.2. Preparation of composite magnetic nanoparticles MNP

Fig. 1B and C shows the TEM and SEM micrographs of MNP (formula C). As it can be noticed, they are spherical with a relatively narrow polydispersity. Magnetite different encapsulated amounts (see different formulas, Table 1) did not show an influence on the MNP size or size distribution. Indeed, some papers (Jun et al., 2005; Pich et al., 2005; Spiers et al., 2006) have shown a polydispersity of magnetite-loaded carriers, increasing with the increase of incorporated magnetite amount. Pich et al. (2005) attributed this polydispersity increase to a simultaneous formation of large polystyrene composite microspheres and smaller ones, with a magnetite core and a polymeric shell, precipitating at the surface of larger spheres during polymerization as agglomerates and changing, by consequence, the overall morphology.

Here, concerning PLLA magnetic nanoparticles, prepared by an emulsion evaporation method, we did not find such a correlation between the magnetite loading and MNP size polydispersity or morphology. Furthermore such surface magnetite agglomerates were not seen regardless of the incorporated magnetite amount (Fig. 1C, formula C, magnetite loading up to ∼20%).

The influence of different emulsification factors was thereafter investigated. The most influencing factor on the MNP size was the stirring speed and to a smaller degree, the polymer concentration. It was found that the higher the stirring speed, the smaller the MNP size and the narrower the size distribution. This trend was also described by Hamoudeh and Fessi (2006) for poly ε-caprolactone (PCL)-based magnetic microparticles prepared

at relatively lower stirring speeds (2000 rpm maximum). For instance, the MNP size ranged from 300 ± 10 to 1300 ± 168 nm at stirring speeds of 24,000 and 6500 rpm, respectively (Fig. 2). This stirring speed influence on nanoparticles size has been largely established in literature. Lee et al. (2005) and Zhang et al. (2006) showed that the higher the stirring speed the smaller the dispersed organic droplets, thus the smaller obtained nanoparticles. The increase in polymer concentration was also found to relatively increase the MNP size, while fixing other parameters, and to induce a larger size polydispersity (Fig. 3). Such effect was also reported in our previous paper (Hamoudeh and Fessi, 2006) using PCL instead of PLLA. Chorny et al. (2002) explained this polymer effect by the fact that at a relatively higher polymer concentration, the organic phase would become more viscous rendering it more resistant to shear forces (Eun Kyoung et al., 2005).

Concerning the PVA concentration in the aqueous phase, no clear influence on the MNP size could be found (data not shown) in contrary with our first study (Hamoudeh and Fessi, 2006). We would explain this difference by two points; firstly, in this new study we used so much higher stirring speeds between
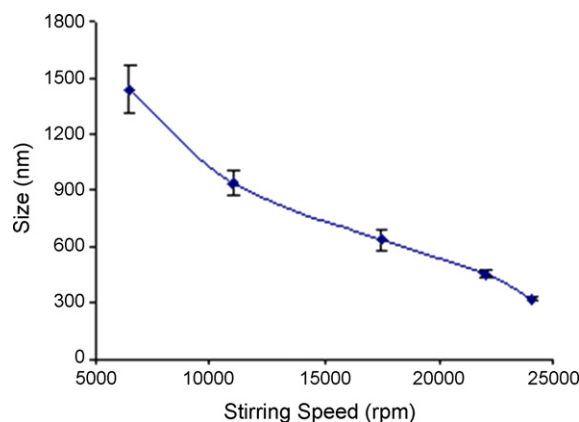
Fig. 2. The stirring speed influence on the MNP size. (Polymer concentration = 4%, w/v and PVA concentration = 0.5%, w/v) (assays were performed in triplicate).
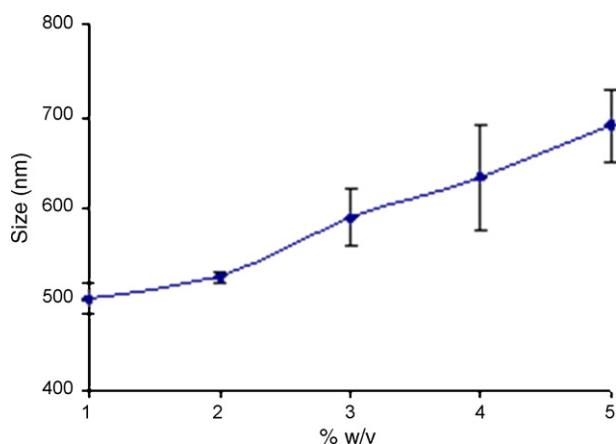
Fig. 3. The PLLA concentration influence on the MNP size. (Stirring speed = 17,500 rpm and PVA concentration = 0.5%, w/v) (assays were performed in triplicate).

Table 2
XPS results of PLLA, PVA and composite magnetic nanoparticles MNP (formula D which has the highest magnetite loading)

Substance	Chemical structure	C (at.%)	O (at.%)	%Fe (at.%)	O/C
PLLA	$(-O-CH(CH_3)CO-)_n$	64.4	35.6	0	0.55
PVA	$(C_2H_4O)_n$	67	33	0	0.50
Magnetite	Fe_3O_4	8.9	69.5	21.6	nd
MNP	–	64	36	<0.1	0.56

6500 and 24,000 rpm against 500 and 2000 rpm in the former one. Secondly, in this study the polymer concentrations and its molecular weight were relatively smaller, between 1 and 5% (w/v) of PLLA (Mw = 6 kDa) instead of 4–12% (w/v) of PCL (Mw = 14 kDa) in the former one. As reported above, both the increase of the stirring speed and the decrease of the polymer concentration in DCM contribute to the reduction of the MNP size. Therefore, getting these two accompanied points in this new study into account, we would think that a potential influence of increased PVA concentration on the MNP size has been effectively masked. Indeed, the PVA-induced particles size reduction has been frequently mentioned in literature (Kwon et al., 2001; Sahoo et al., 2002). Nevertheless, some few papers have shown an absence or a non-significance of such stabilizer effect (Ma and Pa, 2004; Samati et al., 2006).

However, as the residual amount of PVA must be monitored for quality and safety purposes, the colorimetric titration of absorbed PVA into MNP has shown that a less than 2% (w/w) of PVA, which is found also elsewhere (Carrio et al., 1991; Boury et al., 1995; Sahoo et al., 2002; Zambaux et al., 1998). Furthermore, it was found to increase slightly with the PVA amount used in formulation which is in agreement with Sahoo et al. (2002). Indeed, the last cited papers have shown a residual PVA remaining in the composition of the nanoparticles after their preparation with a practical difficulty to eliminate it from the particles surface (Boury et al., 1995).

3.3. Encapsulation efficacy

Both the ICP-AES and the TGA showed that the encapsulation efficiency was around 90% whatever the magnetite/polymer ratio was. We found that about the quasi total magnetite amount used in formulation was well detected experimentally in a reproducible way (Table 2, ICP-AES results). Fig. 4 shows the TGA curve of the different formulas in which it can be noticed that the found amount of iron oxide (at 1000 °C) scaled with the theoretical amount of magnetite (at a polymer concentration of 4%, w/v). Furthermore, the highest magnetite loading that we could obtain was about 30% (w/w) (formula D) correspond-

ing to an encapsulation efficacy of 90% also. Such a magnetic loading in PLLA particles was also mentioned by Spiers et al. (2006) yielding a comparable value of saturation magnetization (Ms = 15 emu/g) being suitable according to authors for a hypothermic treatment of liver cancer. Indeed, the 30% (w/w) magnetite loading in our study should be very sufficient to enable a MRI application in order to use these MNP to detect their distribution within or around the tumor in a trial to optimize a local anticancer treatment.

3.4. X-ray diffraction

As mentioned above, the chemical structure of prepared magnetite was studied by X-ray diffraction. It was shown that the crystalline pattern coincide very well with the standard pattern of magnetite showing an isometric-hexoctahedral crystal system. Fig. 5 shows that the XRD typical spectra of magnetite can be detected in the MNP (formula C) indicating that magnetite structure has not changed during both emulsification and nanoparticles formation (also in the other 3 formulas, data not shown) which is very crucial to keep its magnetic behaviour and relaxivity properties.

3.5. Infrared spectra analysis

Fig. 6 shows the FTIR spectra of MNP (formula C). The characteristic absorption peak for Fe_3O_4 is observed at 580 cm^{-1} in
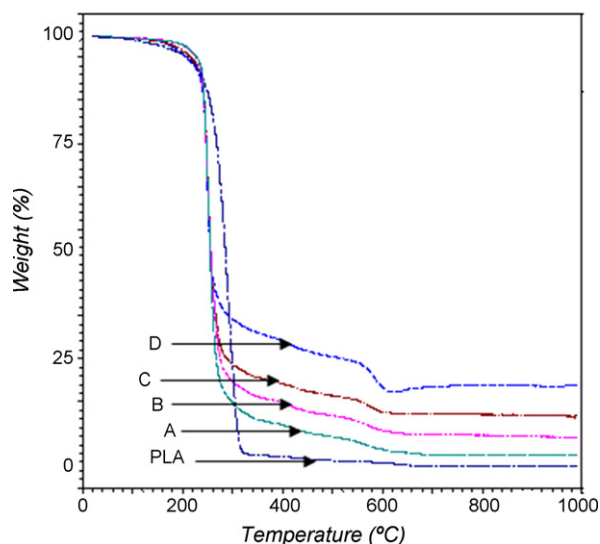
Fig. 4. The TGA analysis of MNP (different formulas).
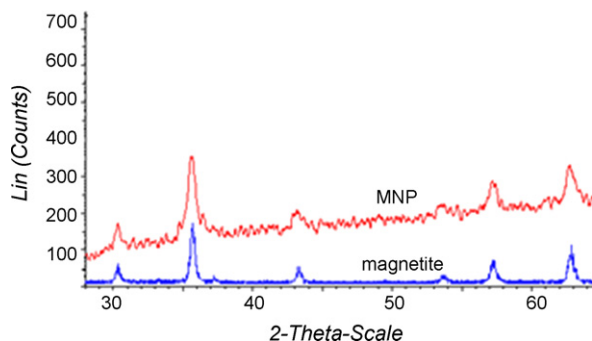
Fig. 5. The XRD of magnetite and MNP (formula C).

agreement with other works (Lee et al., 1996; Yoon et al., 2003; Liu et al., 2006; Wei et al., 2006), and those of the PLLA are evident at about 1750 cm^{-1} (carbonyl groups), 1080 cm^{-1} (C–O–C stretching bands) and 1450 cm^{-1} (C–H stretching in methyl groups) (Lee et al., 1996; Paragkumar et al., 2006). This confirms the encapsulation of magnetite within the matrix of the PLLA.

3.6. Zeta potential determination

It has been mentioned that the surface properties of magnetite are extremely sensitive to pH fluctuations. However, such properties should not be found when magnetite crystals are well encapsulated in the interior of PLLA nanoparticles. Thus, we investigated the influence of pH on the MNP zeta-potential.

In agreement with other papers (Sun et al., 1998; Hamoudeh and Fessi, 2006), synthesized magnetite crystals show an obvious isoelectric point in the vicinity of pH 6.7 accompanied by a negative potential in alkaline pH medium and a positive one in acidic pH medium. Effectively, MNP (for the 4 formulas) and magnetite-free nanoparticles surface charges were not influenced by the pH values (Fig. 7, formula C). Thus, the zeta potential of MNP was found to be less positive (negative) than that of magnetite at acid (basic) pH values. This leads to the confirmation that magnetite is well encapsulated in the interior of MNP.

3.7. XPS

For this assay we have chosen the MNP (formula D) which contains the highest magnetite content. XPS analyses clearly
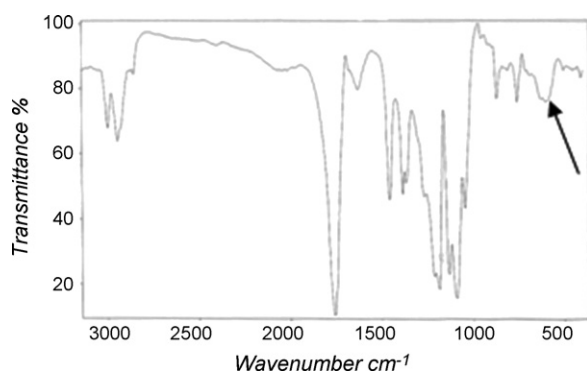
Fig. 6. The FTIR analyses of MNP (formula C). The flesh indicates the characteristic absorption peak for Fe$_3$O$_4$ which is observed at 580 cm^{-1}.
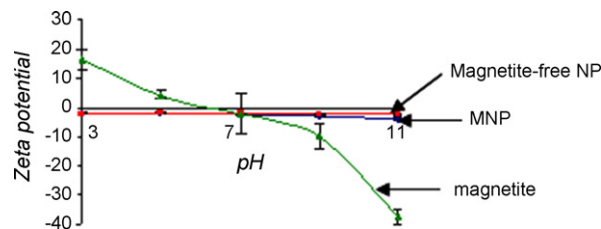
Fig. 7. The pH influence on the MNP zeta potential (formula C), magnetite-free nanoparticles and magnetite (assays were performed in triplicate).

showed the quasi absence of Fe atoms at the surface of MNP (less than 0.1%) indicating the success of the encapsulation of magnetite within the MNP. Furthermore, the high carbon content of MNP is related to the organic structure of the polymer material (Table 2) and in a small but not negligible contribution from PVA. The O/C atomic ratio of PLLA and MNP was found to be 0.56 in accordance with other works (Kiss et al., 2002; Lin et al., 2006). Also, a small amount of carbon atoms was detected at the surface of the magnetite sample coming from a probable contamination due to a short contact with air during XPS sample preparation.

3.8. Magnetic behaviour

As mentioned above (Section 3.1), the saturation magnetization of synthesized magnetite was 70 emu/g being comparable to other works (Xu et al., 2002).

Concerning the MNP, Fig. 8 shows that the saturation magnetization (Ms) at room temperature (300 K) increasing logically with the increase of the encapsulated amount of magnetite within MNP (experimental loading) (see Table 1). The highest obtained (Ms) value was 14 emu/g$_{nanoparticles}$ being equivalent to 88 emu/g$_{iron}$ which is comparable with the known (Ms) of the commercialized contrast agent (Endorem®, Guerbet, France). The presence of the non-magnetic PLLA matrix is evidenced by the fact that (Ms) of composite nanoparticles is much smaller than that of the pure magnetite, and the initial magnetization-field dependence is steeper in the latter case. Nevertheless, the MNP still show a higher saturation magnetization value (Ms) than the ones reported by other research groups (<0.1 emu/g by Lee et al. (2005), 4 emu/g by Wang et al. (2005), 7.3 emu/g by Hu et al. (2006)). Therefore, the relatively high magnetization
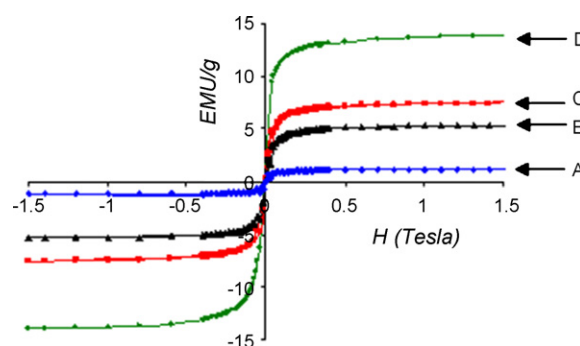
Fig. 8. The magnetic behaviour of MNP (different formulas) at different magnetite loading.
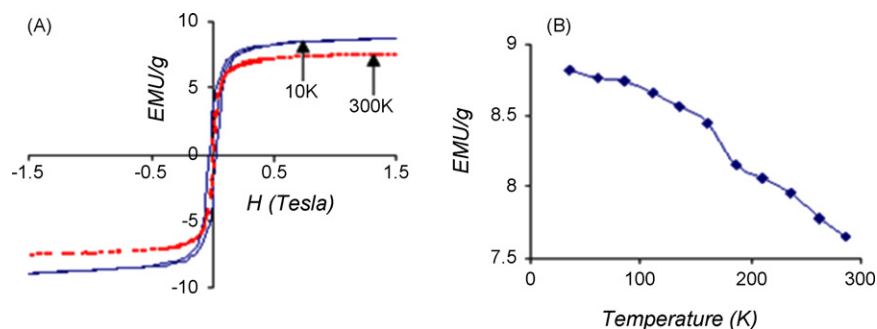
Fig. 9. (A and B) The temperature influence on the MNP magnetisation (formula C).

of our MNP should render them useful from a magnetic vector technology point of view.

Furthermore, we have studied the magnetic behaviour of these MNP at different temperatures but at a fixed magnetic field. Fig. 9A shows the field dependence of MNP magnetization at 10 and 300 K. It can be seen that the MNP exhibit the characteristics of a soft magnetic material, where a characteristic hysteresis is observed at 10 K and disappears with a very negligible both remanence and coercivity (Hc) at 300 K with compliance with other works (Yoon et al., 2003; Wei et al., 2006). Indeed, when the temperature is decreased to 10 K, the magnetization of the sample increases with a symmetric hysteresis loop, showing a transition from superparamagnetic to ferromagnetic behaviour. Such effect indicates the absence of a long-range magnetic dipole–dipole interaction among the material of these nanoparticles at 300 K. Thus, the nanoparticles display superparamagnetic characteristic, indicating that the MNP do obey a single-domain theory above the blocking temperature, a phenomenon which was expected due to the very small and homogenous diameter of synthesized magnetite; 12 nm as found in TEM images. Indeed, the critical particle size of ferromagnetism of magnetite is known to be 25 nm, based on theoretical calculation from the equation $KV \sim 25 \, kT$, where k, T, K, and V are the Boltzmann constant, the absolute temperature, anisotropy constants, and the particle volume, respectively (Wei et al., 2006).

Furthermore, Fig. 9B shows the MNP magnetic saturation moment (Ms) (formula C) decreasing as the temperature increases from 35 to 300 K at the applied magnetic field of 1.5 T, an effect which has been also reported in other works in the literature (Yoon et al., 2003; Wei et al., 2006).

3.9. In vitro relaxivity

The iron concentration in different tubes was varied between 0 and 0.75 mM. The T_1 relaxation time decreased from 1168 to 586 ms at concentrations ranging between 0.05 and 0.75 mM. The calculated r_1 relaxivity by the IR-FISP cartography map was $1.7 \pm 0.1 \, s^{-1} \, mM^{-1}$. This value is in accordance with the reported data concerning commercialized contrast agent of the family of superparamagnetic iron oxides (SPIO) as Endorem® (Guerbet, France) ($r_1 = 2.3 \, s^{-1} \, mM^{-1}$) at the same magnetic field (Rohrer et al., 2005).

MSME T_2-weighted images of MNP with the same iron concentrations are shown in Fig. 10. On T_2-weighted
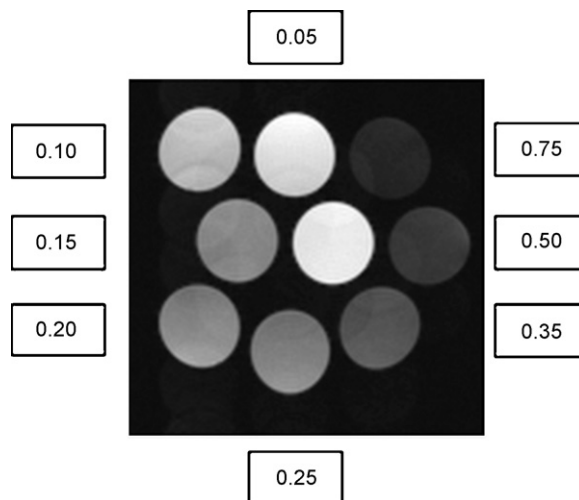
Fig. 10. T_2-weighted image of MNP at different iron concentrations (mM). The tube in the centre has 0% mM iron.

images, the presence of MNP induced an increased signal lose with the increase of iron concentration. The T_2 relaxation time decreased from 52 to 7 ms at concentrations ranging between 0.05 and 0.75 mM. The calculated r_2 relaxivity was $228.3 \pm 13.1 \, s^{-1} \, mM^{-1}$. Indeed, the enhancement of r_2 relaxivity reflects the ability of these MNP to locally disturb the magnetic field around the particles and through which water molecules diffuse inducing dephasing of the proton magnetic moments and as a consequence a T_2 effective relaxation shortening. Compared to the transverse relaxivity of Endorem® ($r_2 = 105 \, s^{-1} \, mM^{-1}$) at the same magnetic field, the relatively higher r_2 value of these MNP renders them particularly suitable to be used as negative MR contrast agent in T_2-weighted imaging. Thus, if an anti-cancerous drug is encapsulated within these MNP before their preparation, these nanoparticles could be very useful in controlling the drug distribution within a tumor mass, after a local intra-tumoral injection, under the supervision of a medical staff equipped with MRI facilities. Due to such medical monitoring, their utilization is expected to improve the anti-tumoral treatment efficacy and to reduce treatment induced side effects.

4. Conclusion

This paper approaches the incorporation of magnetite in polymer-based nanoparticles for a medical application based

on magnetic properties. Magnetite has been prepared by a coprecipitation method in alkaline pH medium. Synthesized magnetite crystals were characterized by X-ray diffraction and showed to have the standard crystalline structure of magnetite and a nanometric size of 12 nm. The magnetite encapsulation within magnetic nanoparticles MNP, was applied by an emulsion evaporation method. The encapsulation efficacy, measured by thermogravemetric analysis and ICP-AES was more than 90% yielding a high magnetite yield of up to 30% (w/w). The X-ray photoelectron spectroscopy (XPS) assay for MNP showed less than 0.1% of iron atoms at the nanoparticles surface which was also supported by the zeta potential response of MNP towards pH variation giving evidence of the success of the magnetite encapsulation in the interior of MNP. The prepared MNP have superparamagnetic behaviour with a saturation magnetization increasing with the increased magnetite amount used in formulation. Furthermore, the in vitro MRI study showed that these MNP had a very good T_2 relaxivity of $228\,\mathrm{s}^{-1}\,\mathrm{mM}^{-1}$ rendering them practically useful as a negative contrast agent for MRI. Thus, these magnetic nanoparticles can be very interesting for magnetic resonance imaging (MRI) to control the drug delivery localisation after a local administration in tumors yielding a better treatment efficacy and lesser treatment induced side effects.

Acknowledgment

References

Bonnemain, B., 1998. Superparamagnetic agents in magnetic resonance imaging: physicochemical characteristics and clinical applications. J. Drug Target 6, 167–174.

Boury, F., Ivanova, T.Z., Panaıotov, I., Proust, J.E., Bois, A., Richou, J., 1995. Dynamic properties of poly(DL-lactide) and polyvinyl alcohol monolayers at the air/water and dichloromethane/water interfaces. J. Colloid Interface Sci. 169, 380–392.

Carrio, A., Schwach, G., Coudane, J., Vert, M., 1991. Preparation and degradation of surfactant-free PLAGA microspheres. J. Control. Release 37, 113–121.

Chiang, C.L., Sung, C.S., 2006. Purification of transfection-grade plasmid DNA from bacterial cells with superparamagnetic nanoparticles. J. Magn. Magn. Mater. 302, 7–13.

Chorny, M., Fishbein, I., Danenberg, H.D., Golomb, G.J., 2002. Lipophilic drug loaded nanospheres prepared by nanoprécipitation. Effect of formulation variables on size, drug recovery and release kinetics. Control. Release 83, 389–400.

Deng, Y., Wang, L., Yang, W., Fu, S., Elaıssari, A., 2003. Preparation of magnetic polymeric particles via inverse microemulsion polymerization process. J. Magn. Magn. Mater. 257, 69–78.

Eun Kyoung, P., Sang Bong, L., Young Moo, L., 2005. Preparation and characterization of methoxy poly(ethylene glycol)/poly(ε-caprolactone) amphiphilic block copolymeric nanospheres for tumor-specific folate-mediated targeting of anticancer drugs. Biomaterials 26, 1053–1061.

Go, K.G., Bulte, J.W., De Ley, L., The, T.H., Kamman, R.L., Hulstaert, C.E., Blaauw, E.H., Ma, L.D., 1993. Our approach towards developing a specific tumor-targeted MRI contrast agent for the brain. Eur. J. Radiol. 16, 171–175.

Gomez-Lopera, S.A., Plaza, R.C., Delgado, A.V., 2001. Synthesis and characterization of spherical magnetite/biodegradable polymer composite particles. J. Colloid Interface Sci. 240, 40–47.

Gupta, A.K., Gupta, M., 2005. Synthesis and surface engineering of iron oxide nanoparticles for biomedical applications. Biomaterials 26, 3995–4021.

Hafeli, U.O., Sweeney, S.M., Beresford, B.A., Sim, E.H., Macklis, R.M., 1994. Magnetically directed poly(lactic acid) 90Y-microspheres: novel agents for targeted intracavitary radiotherapy. J. Biomed. Mater. Res., 901–908.

Hamoudeh, M., Fessi, H., 2006. Preparation, characterization and surface study of poly-epsilon caprolactone magnetic microparticles. J. Colloid Interface Sci. 300, 584–590.

Herrmann, J., Bodmeier, R., 1998. Biodegradable, somatostatin acetate containing microspheres prepared by various aqueous and non-aqueous solvent evaporation methods. Eur. J. Pharm. 45, 75–82.

Hu, F.X., Neoh, K.G., Kang, E.T., 2006. Synthesis and in vitro anti-cancer evaluation of tamoxifen-loaded magnetite/PLLA composite nanoparticles. Biomaterials 27, 5725–5733.

Jun, J.B., Uhm, S.Y., Ryu, J.H., Suh, K.D., 2005. Synthesis and characterization of monodisperse magnetic composite particles for magnetorheological fluid materials. Colloid Interface 260, 157–164.

Kim, D.K., Zhang, Y., Voit, W., Rao, K.V., Kehr, J., Bjelke, B., Muhammed, M., 2001. Superparamagnetic iron oxide nanoparticles for bio-medical applications. Scr. Mater. 44, 1713–1717.

Kim, D.H., Lee, S.H., Im, K.H., Kim, K.N., Kim, K.M., Shim, I.B., Lee, M.H., Lee, Y.K., 2006. Surface-modified magnetite nanoparticles for hyperthermia: preparation, characterization, and cytotoxicity studies. Curr. Appl. Phys. 6, e242–e246.

Kiss, E., Bertóti, I., Vargha-Butler, E.I., 2002. XPS and wettability characterization of modified poly(lactic acid) and poly(lactic/glycolic acid) films. J. Colloid Interface Sci. 245, 91–98.

Kryszewski, M., Jeszka, J.K., 1998. Nanostructured conducting polymer composites- superparamagnetic particles in conducting polymers. Synth. Metals 94, 99–104.

Kwon, H.Y., Lee, J.Y., Choi, S.W., Kim, J.H., 2001. Preparation of PLGA nanoparticles containing estrogen by emulsification–diffusion method. Colloid Surf. A 182, 123–130.

Lee, J., Isobe, T., Senna, M., 1996. Preparation of ultrafine Fe_3O_4 particles by precipitation in the presence of PVA at high pH. J. Colloid Interface Sci. 177, 490–494.

Lee, S.J., Jeong, J.R., Shin, S.C., Kim, J.C., Chang, Y.H., Lee, K.H., Kim, J.D., 2005. Magnetic enhancement of iron oxide nanoparticles encapsulated with poly(D,L-latide-co-glycolide). Colloids Surf. A 255, 19–25.

Lemoine, D., Francois, C., Kedzierewicz, F., Preat, V., Hoffman, M., Maincent, P., 1996. Stability study of nanoparticles of poly(ε-caprolactone), poly(D,L-lactide) and poly(D,L-lactide-co-glycolide). Biomaterials 17, 2191–2197.

Lin, Y.S., Ho, T.L., Chiou, L.H., 1986. Microencapsulation and controlled release of insulin from polylactic acid microcapsules. Biomater. Med. Devices Artif. Organs 13, 187–201.

Lin, Y., Wang, L., Zhang, P., Wang, X., Chen, X., Jing, X., Su, Z., 2006. Surface modification of poly(L-lactic acid) to improve its cytocompatibility via assembly of polyelectrolytes and gelatine. Acta Biomaterialia, 155–164.

Liu, X., Kaminski, M.D., Guan, Y., Chen, H., Liu, H., Rosengart, A.J., 2006. Preparation and characterization of hydrophobic superparamagnetic magnetite gel. J. Magn. Magn. Mater. 306, 248–253.

Ma, Z., Pa, P.L., 2004. Dispersion polymerization of 2-hydroxyethyl methacrylate stabilized by a hydrophilic/CO_2-philic poly(ethyleneoxide)-b-poly(1,1,2,2-tetrahydroperfluorodecyl acrylate) (PEO-b-PFDA) diblock copolymer in supercritical carbon dioxide. Polymer 45, 6789–6797.

Maensiri, S., Laokul, P., Klinkaewnarong, J., 2006. A simple synthesis and room-temperature magnetic behavior of Co-doped anatase TiO_2 nanoparticles. J. Magn. Magn. Mater. 302, 448–453.

Müller, R.H., Maassen, S., Weyhers, H., Specht, F., Lucks, J.S., 1996. Cytotoxicity of magnetite-loaded polylactide/glycolide particles and solid lipid nanoparticles. Int. J. Pharm. 138, 85–94.

Okassa, L.N., Marchais, H., Douziech-Eyrolles, L., Cohen-Jonathan, S., Soucé, M., Dubois, P., Chourpa, I., 2005. Development and characterization of sub-micron poly(d,l-lactide-co-glycolide) particles loaded with magnetite/maghemite nanoparticles. Int. J. Pharm. 302, 187–196.

Paragkumar, I.N.T., Edith, D., Six, J.L., 2006. Surface characteristics of PLLA and PLGA films. Appl. Surf. Sci. 253, 2758–2764.

Pauser, S., Reszka, R., Wagner, S., Wolf, K.J., Buhr, H.I., Berger, G., 1997. Liposome-encapsulated superparamagnetic iron oxide particles as markers in an MRI-guided search for tumor-specific drug carriers. Anticancer Drug Des. 12, 125–135.

Pich, A., Bhattacharyaa, S., Ghoshb, A., Adler, H.J.P., 2005. Composite magnetic particles: encapsulation of iron oxide by surfactant-free emulsion polymerization. Polymer 46, 4596–4603.

Rohrer, M., Bauer, H., Mintorovitch, J., Requardt, M., Weinmann, H.J., 2005. Comparison of magnetic properties of MRI contrast media solutions at different magnetic field strengths. Invest. Radiol. 40, 715–724.

Roullin, V.G., Deverre, J.R., Lemaire, L., Hindré, F., Venier-Julienne, M.C., Vienet, R., Benoit, J.P., 2002. Anti-cancer drug diffusion within living rat brain tissue: an experimental study using [3H](6)-5-fluorouracil-loaded PLGA microspheres. Eur. J. Pharm. Biopharm. 53, 293–299.

Safaiikova, M., Roy, I., Gupta, M.N., Safaiik, I., 2003. Magnetic alginate microparticles for purification of α-amylases. J. Biotech. 105, 255–260.

Sahoo, S.K., Panyam, J., Prabha, S., Labhasetwar, V., 2002. Residual polyvinyl alcohol associated with poly (D,L-lactide-co-glycolide) nanoparticles affects their physical properties and cellular uptake. J. Control. Release 82, 105–114.

Samati, Y., Yüksel, N., Tarimci, N., 2006. Preparation and characterization of poly(D,L-lactic-co-glycolic acid) microspheres containing flurbiprofen sodium. Drug Delivery 13, 105–111.

Seppenwoolde, J.H., Nijsen, J.F., Bartels, L.W., Zielhuis, S.W., Van Het Schip, A.D., Bakker, C.J., 2005. Internal radiation therapy of liver tumors: qualitative and quantitative magnetic resonance imaging of the biodistribution of holmium-loaded microspheres in animal models. Magn. Reson. Med. 53, 76–84.

Shieh, D.B., Cheng, F.Y., Su, C.H., Yeh, C.S., Wu, M.T., Wu, Y.N., Tsai, C.Y., Wu, C.L., Chen, D.H., Chou, C.H., 2005. Aqueous dispersions of magnetite nanoparticles with NH_3+ surfaces for magnetic manipulations of biomolecules and MRI contrast agents. Biomaterials 26, 7183–7191.

Sindhu, S., Jegadesan, S., Parthiban, A., Valiyaveettil, S., 2006. Synthesis and characterization of ferrite nanocomposite spheres from hydroxylated polymers. J. Magn. Magn. Mater. 296, 104–113.

Spiers, K.M., Forsythe, J.S., Suzuki, K., Cashion, J.D., 2006. Production of magnetic microspheres by ultrasonic atomisation. J. Magn. Magn. Mater. (Online).

Sun, Z.X., Su, F.W., Forsling, W., Samskog, P.O., 1998. Surface characteristics of magnetite in aqueous suspension. J. Colloid Interface Sci. 197, 151–159.

Timko, M., Koneracka, M., Tomas ovicova, N., Kopcansky, P., Zcvisova, V., 2006. Magnetite polymer nanospheres loaded by Indomethacin for anti-inflammatory therapy. J. Magn. Magn. Mater. 300, e191–e194.

Ushakova, M.A., Chernyshev, A.V., Taraban, M.B., Petrov, A.K., 2003. Observation of magnetic field effect on polymer yield in photoinduced dispersion polymerization of styrene. Eur. Polymer J. 39, 2301–2306.

Wang, Y.X.J., Hussain, S.M., Kresting, G.P., 2001. Superparamagnetic iron oxide contrast agents: physicochemical characteristics and applications in MR imaging. Eur. Radiol. 11, 2319–2331.

Wang, P.C., Lee, C.F., Young, T.H., Lin, D.T., Chiu, W.Y., 2005. Preparation and clinical application of immunomagnetic latex. J. Polym. Sci., Part A, Polym. Chem. 43, 1342–1356.

Wassel, R.A., Grady, B., Kopke, R.D., Dormer, K.G., 2007. Dispersion of super paramagnetic iron oxide nanoparticles in poly(D,L-lactide-co-glycolide) microparticles. Colloids Surf. A 292, 125–130.

Wei, S., Zhu, Y., Zhang, Y., Xu, J., 2006. Preparation and characterization of hyperbranched aromatic polyamides/Fe_3O_4 magnetic nanocomposite. React. Funct. Polym. 66, 1272–1277.

Weissleder, R., Elizondo, G., Wittenberg, J., Rabito, C.A., Bengele, H.H., Josephson, L., 1990. Ultrasmall superparamagnetic iron oxide: characterization of a new class of contrast agents for MR imaging. Radiology 175, 489–493.

Xie, X., Zhang, X., Zhang, H., Chen, D., Fei, W.Y., 2004. Preparation and application of surface-coated superparamagnetic nanobeads in the isolation of genomic DNA. J. Magn. Magn. Mater. 277, 16–23.

Xu, X., Friedman, G., Humfeld, K.D., Majetichi, S.A., Asher, S.A., 2002. Synthesis and utilization of monodisperse superparamagnetic colloidal particles for magnetically controllable photonic crystals. Chem. Mater. 14, 1249–1256.

Yoon, M., Kim, Y.M., Kim, Y., Volkov, V., Song, H.J., 2003. Magnetic properties of iron nanoparticles in a polymer film. J. Magn. Magn. Mater. 265, 357–362.

Zambaux, M.F., Bonneaux, F., Gref, R., Maincent, P., Dellacherie, E., Alonso, M.J., Labrude, P., Vigneron, C., 1998. Influence of experimental parameters on the characteristics of poly(lactic acid) nanoparticles prepared by a double emulsion method. J. Control. Release 50, 31–40.

Zhang, J.Y., Shen, Z.G., Zhong, J., Hu, T.T., Chen, J.F., Ma, Z.Q., Yun, J., 2006. Preparation of amorphous cefuroxime axetil nanoparticles by controlled nanoprecipitation method without surfactants. Int. J. Pharm. 323, 153–160.

Zheng, W., Gao, F., Gu, H., 2005. Magnetic polymer nanospheres with high and uniform magnetite content. J. Magn. Magn. Mater. 288, 403–410.

Zielhuis, S.W., Nijsen, J.F.W., Figueiredo, R., Feddes, B., Vredenberg, A.M., Van het Schip, A.D., Hennink, W.E., 2005a. Surface characteristics of holmium-loaded poly(L-lactic acid) microspheres. Biomaterials 26, 925–932.

Zielhuis, S.W., Nijsen, J.F., Seppenwoolde, J.H., Zonnenberg, B.A., Bakker, C.J., Hennink, W.E., Van Rijk, P.P., Van het Schip, A.D., 2005b. Lanthanide bearing microparticulate systems for multi-modality imaging and targeted therapy of cancer. Curr. Med. Chem. Anticancer Agents 5, 303–313.